Solution Processed Polymer-ABX$_4$ Perovskite-Like Microcavities

Paola Lova [1], **Daniele Cortecchia [2,3]**, **Cesare Soci [4,***] and **Davide Comoretto [1,***]**

[1] Dipartimento di Chimica e Chimica Industriale, Università degli Studi di Genova, Via Dodecaneso 31, 16146 Genova, Italy; paola.lova@edu.unige.it

[2] Energy Research Institute @ NTU (ERI@N), Interdisciplinary Graduate School, Nanyang Technological University, 50 Nanyang Drive, Singapore 637553, Singapore; Daniele.Cortecchia@iit.it

[3] Centre for Nano Science and Technology (CNST@PoliMi), Istituto Italiano di Tecnologia, Via Pascoli 70, 20133 Milan, Italy

[4] Centre for Disruptive Photonic Technologies, TPI, SPMS, Nanyang Technological University, 21 Nanyang Link, Singapore 637371, Singapore

* Correspondence: csoci@ntu.edu.sg (C.S.); davide.comoretto@unige.it (D.C.)

Featured Application: Solution processed perovskite-polymer microcavities can find applications in lightening devices such as LEDs and in lasing.

Abstract: Thanks to solution processability and broad emission in the visible spectral range, 2D hybrid perovskite-like materials are interesting for the realization of large area and flexible lighting devices. However, the deposition of these materials requires broad-spectrum solvents that can easily dissolve most of the commercial polymers and make perovskites incompatible with flexible photonics. Here, we demonstrated the integration of broadband-emitting (EDBE)PbCl$_4$ (where EDBE = 2,2-(ethylenedioxy)bis(ethylammonium)) thin films with a solution-processed polymer planar microcavities, employing a sacrificial polymer multilayer. This approach allowed for spectral and angular redistribution of the perovskite-like material, photoluminescence, that can pave the way to all-solution-processed and flexible lightning devices that do not require complex and costly fabrication techniques.

1. Introduction

Hybrid perovskites garnered increasing interest due to the ease of engineering their optoelectronic properties via simple wet chemistry and to the good power conversion efficiencies achieved in photovoltaics [1–10]. Successively, the solution processability of these materials has opened up new perspectives on abiding costs and simplifying fabrication processes for lightening and optoelectronic devices such as light emitting diodes and solid-state lasers [11–18], whilst maintaining the ease of tunability of the emission properties. Among these, perovskite-like material with 2D lattices, such as 2,2'-(ethylenedioxy)bis(ethylammonium) lead chloride (EDBE)PbCl$_4$, became interesting thanks to its broad photoluminescence spectrum, which ranges from the ultraviolet to the near infrared and gives to this material its characteristic broad photoluminescence [19–27]. These characteristics arise from the 2D structures in which the large organic molecule allows for the formation of a lamellar crystalline structures where planes of lead chloride are alternated to planes of 2,2'-(ethylenedioxy)bis(ethylammonium) [19,20]. These materials are promising for light-emitting devices coupled to photonic structure to engineer their emission [11,20,28–30]. Photonic crystals have indeed been widely employed to engineer the emission

of photoactive materials [31–34]. Among the large variety of photonic structures demonstrated in recent decades, spun-cast planar microcavities and distributed Bragg reflectors (DBRs) are a viable and low-cost approach to this task thanks to solution processing and the large availability of polymer media [35]. These structures consist of dielectric lattices made of thin film with different refractive indexes, alternated periodically, that interact with light generating specific frequency regions forbidden photon propagation, namely photonic band gaps (PBGs). Microcavities and DBRs were demonstrated for several applications including photon recycling in photovoltaics [36], sensing [35,37–42] and optical switchers [43–45]. With regards to emission control, these planar lattices are of interest thanks to the spectral and directional redistribution of the photoluminescence oscillator strength [46], as already demonstrated for polymers and organic dyes [47–55] as well as inorganic emitters [54,56]. To control emitted light, the photoactive material can be placed within an engineered defect in the planar lattice [47,49], or it can be used as an active component of the photonic crystal lattice itself [48,57,58]. These two strategies favor emission enhancement from the cavity mode or band edge, respectively. Unfortunately, as with most solution-processable perovskites, $(EDBE)PbCl_4$ can only be casted from broad-spectrum solvents such as dimethylformamide (DMF) and dimethyl sulfoxide (DMSO), which are solvents for most of the commercial polymers, thus making mutual processing of polymer photonic structures and perovskites incompatible. To circumvent these limitations, in a previous work, we coupled white emitting $(EDBE)PbCl_4$ thin films casted on fused silica or thick polyethylene terephthalate substrates, with DBRs that where successively grown on top of the perovskite layer to create half microcavities able of emission enhancement and suppression [21]. Successively, we were able to embed a perovskite thin film as a cavity layer within a polymer microcavity, achieving a Q factor of 155 and employing perfluorinated protective layers to avoid the dissolution of the underlying polymer photonic structure during the $(EDBE)PbCl_4$ deposition [59,60]. In this case, the use of a perfluorinated compound as a protective layer complicated the fabrication processes. Indeed, as previously demonstrated, the low wettability of perfluorinated thin films makes complex surface activation processes critical for the fabrication of multilayered structures. [38] In this work, we integrated $(EDBE)PbCl_4$ in a planar polymer photonic structure made of two commodity polymers (polystyrene (PS) and cellulose acetate (CA)), employing part of the underlying DBR as a sacrificial layer. Notwithstanding the fact that this layer was dissolved during the $(EDBE)PbCl_4$ deposition by a DMSO-based precursor solution, the resulting structure could reshape the perovskite-like material emission and enhance its intensity.

2. Materials and Methods

(EDBE)Cl2 was synthetized by a reaction of 2,2′ (ethylenedioxy)bis(ethylamine) (98%, Sigma Aldrich) with two equivalents of HCl (57% w/w in water, Sigma Aldrich) for 2 h at 0 °C. The resulting compound was purified by three cycles of dissolution in hot ethanol and reprecipitation with diethyl ether. The compound was then dried with a rotary evaporator and in vacuum oven overnight at 60 °C. $(EDBE)PbCl_4$ thin films were spun-cast at 4000 RPM for 60 s from a 0.1 M solution prepared by mixing stoichiometric amounts of $(EDBE)Cl_2$ and $PbCl_2$ (99.999% trace metal basis, Aldrich) in dimethyl sulfoxide (anhydrous DMSO, Sigma Aldrich). The resulting films were annealed on a hotplate at 100 °C for 15 min. The $(EDBE)PbCl_4$ deposition was performed in glovebox under N_2 environment.

The polymer microcavities and DBRs were grown on top of quartz substrates by the dynamic spin coating of alternate layers of polystyrene (Mw = 200,000; refractive index, n = 1.58) dissolved in toluene and cellulose acetate (Mw = 61000, n = 1.46) dissolved in diacetone alcohol. The polymer concentrations were ~17 mg/mL for cellulose acetate and 35 mg/ml for polystyrene, and the rotation speed was kept between 4000 and 8000 RPM. After the deposition of the sacrificial half microcavity, a thin $(EDBE)PbCl_4$ film was casted as previously described. After the $(EDBE)PbCl_4$ deposition, a second DBR was spun-cast to complete the structures.

The $(EDBE)PbCl_4$ film thickness and surface roughness were determined by atomic force microscopy (AFM) using a Scanning Probe Microscope Digital Instrument Dimension V.

Angle resolved transmittance and photoluminescence spectra were contemporarily collected, coupling a Fluorolog Horiba endowed with a CCD detector with an Avantes AvaSpec-3046 spectrometer (200–1150 nm, resolution 1.4 nm). Photoluminescence spectra were collected in the range of 390–640 nm using the CCD, with excitation at 335 nm. The transmittance spectra calculated in Figure 3c were simulated using a transfer matrix (TMM) formalism as previously described [21,35], using a Matlab®home-made software (R2017b). The material refractive indexes used as inputs were previously measured and reported in [21,49], while the thickness of the single layers was used as a fitting parameter, retrieving values for CA and PS of 75 nm and 115 nm, respectively. The TMM formalism employed is described in detail in [21,35].

3. Results and Discussion

Figure 1 reports the absorbance and photoluminescence spectra of a 40 nm thin film of $(EDBE)PbCl_4$ casted on fused silica as described in the previous section. The material shows a sharp excitonic absorption peak in the ultraviolet part of the spectrum at 360 nm, while it is transparent in the visible range (Figure 1a). The layered structure of $(EDBE)PbCl_4$ enhances the exciton-phonon coupling, favoring the formation of self-trapped excitons whose radiative decay results in a largely Stokes-shifted, broad emission ranging from the UV to the NIR spectral range. [26] The emission does indeed peak in the green region of the spectrum and ranges from 380 nm to above 600 nm (red line in Figure 1a). In Figure 1b, we report the AFM micrograph of an $EDBE(PbCl_4)$ film casted on a flat fused silica substrate, showing a thickness of about 40 nm and a roughness RMS below 5 nm, as reported in previous researches for film casted under the same condition [20,21].
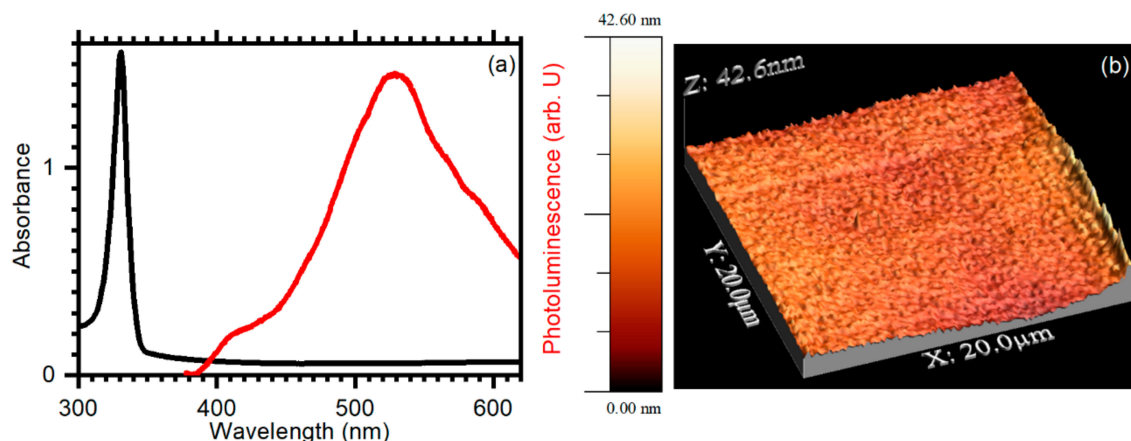

Figure 1. (**a**) $(EDBE)PbCl_4$ absorbance (black line) and photoluminescence (red line) spectra. (**b**) atomic force microscopy (AFM) micrograph of an $(EDBE)PbCl_4$ thin film with thickness of 40 nm deposited on fused silica substrate.

Embedding a $(EDBE)PbCl_4$ thin film into PS:CA multilayered structures, much like the one depicted in Figure 2, favors the formation of colored surfaces. Notwithstanding the deposition of the $(EDBE)PbCl_4$ film, dissolving part of the sacrificial DBR underneath, the samples are still characterized by a vivid color typical of photonic structures. Figure 2 a and c shows the schematic and transmittance spectra of a half microcavity (before the $(EDBE)PbCl_4$ deposition), with PBG tuned into the green part of the spectrum and of the entire microcavity. The spectra were collected at eight different points of a sample. The panel c shows that the DBR (schematized in the panel of the same figure) is homogenous and that the spectra are indeed almost superimposable and present a minimum at about 530 nm, corresponding to the PBG. Moreover, the background is dominated by a Fabry–Pérot interference pattern allowed by partial light reflection at the external interfaces of the half microcavity which attests the good structure optical quality. After the deposition of $(EDBE)PbCl_4$ and the upper half microcavity, we noticed that the spectrum of the sample undergoes several variations (Figure 2b,d). The presence of

the (EDBE)PbCl$_4$ causes a minimum in the transmission spectrum at about 340 nm, corresponding to the (EDBE)PbCl$_4$ excitonic absorption (see Figure 1a). Concerning the feature previously assigned to the PBG, we noticed that it appears inhomogeneously broadened, while its intensity remains roughly unchanged with respect to the half microcavity previously discussed. In this peak, a cavity mode is detected on the long wavelength side (indicated by a black arrow in Figure 2b). This feature arises from the insertion of a defect layer within the photonic crystals, introducing a peak in the density of photonic states within the PBG and allowing photon propagation [35]. Notice that the background of the spectra does not show any clear interference pattern. This characteristic indicates the presence of disorder and light scattering, as can be also evidenced by the digital photographs of the microcavities shown in the inset of Figure 2d. Such disorder derives from the deposition of the (EDBE)PbCl$_4$ layer from the DMSO solution that partially dissolves the underlying sacrificial layers and introduces disorder in the DBR structure. Aside from these effects, the microcavity retained a good quality. This represents the first report of a polymer microcavity obtained without the use of any protective layer of the polymer structure, thus avoiding additional protective films made by expensive and complex processing polymers.
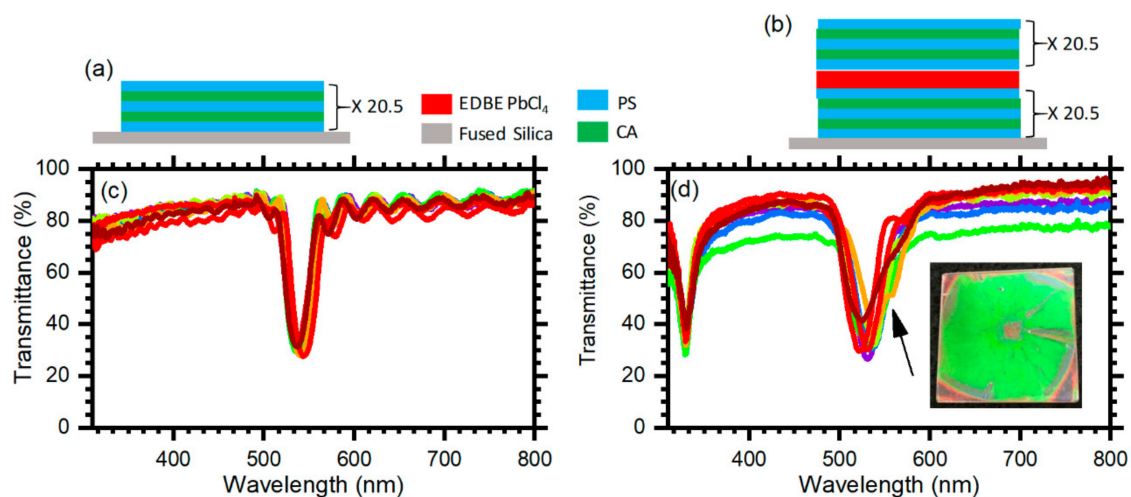

Figure 2. Schematic (**a**,**b**) and transmittance spectra (**c**,**d**) of a polymer half microcavity (**a**,**c**) and of a microcavity where the defect layer consist in an EDBE PbCl$_4$ thin film (**b**,**d**). The inset of panel (**d**) is a digital photograph of the microcavity.

Employing a start-to-end solution processing method allowed us to easily modify structure properties by simple variation of the deposition conditions such as spin-coating rotation speed and concentration of the polymer solution. To better overlap the maxim emission intensity of (EDBE)PbCl$_4$ and PBG, we tuned the latter at 545 nm, a slightly larger wavelength with respect to the sample described above, and the cavity mode at 515 nm, on the short wavelength side of the PBG feature (Figure 3a). Such variations were achieved by decreasing the rotation speed during the deposition of the polymer thin films. The transmittance spectrum of Figure 3a confirms the reproducibility of the fabrication processes, in fact, in both the samples, transmittance values at the PBG are comparable, and the background appears affected by light diffusion, as indicated by the low transmittance values and by the lack of interference fringes. Figure 3a displays the fluorescence spectrum of (EDBE)PbCl$_4$ embedded in the microcavity (red line). By comparison with the spectrum of Figure 1a, we noticed a sharpening of the emission centered at around 515 nm, which corresponds to the cavity mode spectral position. To prove that this effect is assigned to spectral redistribution operated by the photonic band structure, the black line of Figure 3b shows the ratio spectrum obtained, normalizing the data reported in Figure 3a by the emission of the bare (EDBE)PbCl$_4$ thin film. There, the data display a clear enhancement (PLMC/PLREF > 1) at wavelengths corresponding to the cavity mode. To further confirm this interpretation, we collected angular resolved transmittance and photoluminescence spectra

(Figure 3c,d, respectively). Figure 3c shows that the features assigned to the PBG display the angular dispersion expected from theory [35]. In the plot, the x-axis represents the wavelength, while the y-axis represents the angle. The intensity scale is instead reported as a color code for the experimental data so that low intensities appear in red shades while high transmittance values appear in blue shades. The same plot also reports the transmittance calculated via TMM (see Methods section). In this case, only the intensity profile set at transmittance 75% is depicted as a black line in the plot. Experimental and calculated data are in full agreement. Indeed, the PBG is initially detected at 540 nm. When increasing the angle of incidence, it shifts toward the shorter wavelengths in both experimental and calculated data. The panel d of the same figure reports the photoluminescence spectra collected at different angles. We can still notice the broad (EDBE)PbCl$_4$ signal observed in Figure 1b, but in all of the spectra, we found a sharper peak with enhanced intensity moving to the shorter wavelength form 515 nm, for the spectrum collected at 10°, to 460 nm for the one collected at 50°. This is confirmed by the normalized spectra of Figure 3b. The dashed lines that connect panels c and d in Figure 3 guide the eye from the cavity mode detected in the transmittance spectra to the enhanced peak detected in the PL spectra. Such peaks fall on the short wavelength side of the PBG, where the cavity mode is detected, further confirming that the features observed in Figure 3a are assigned to spectral redistribution.
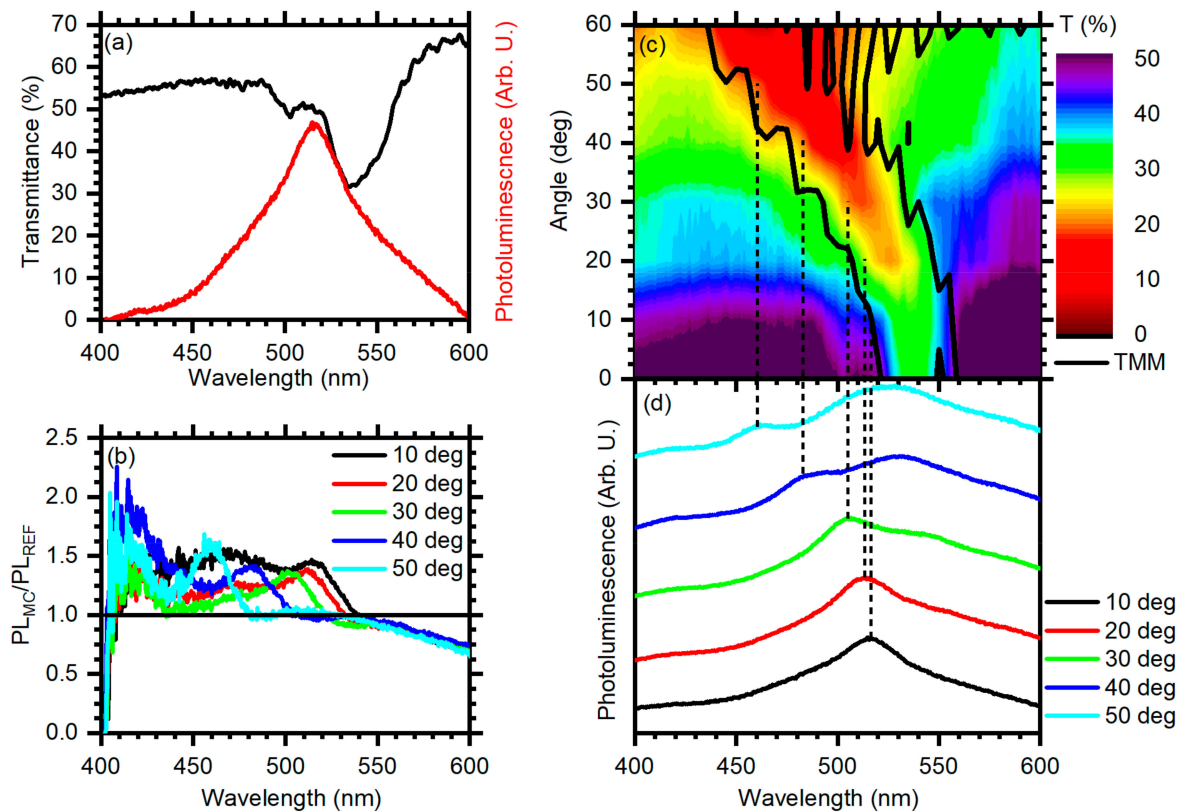

Figure 3. Comparison between the microcavity transmittance (black line) and photoluminescence spectra (red line) collected at 10° (**a**) and 40° (**b**). (**c**) Full angular dispersion of the microcavity transmittance spectrum. The color scale represents the intensity of the experimental data, while the black line is the calculated spectral dispersion of the PBG [35]. (**c**) Photoluminescence spectra collected for different detection angles. The dashed lines connect the enhanced peak (panel **b**) with the cavity mode panel (**c**). (**d**) Photoluminescence ratio spectra obtained normalizing the microcavity emission spectra by the emission spectra of the bare (EDBE)PbCl$_4$ film.

For the data reported in Figure 3, it is possible to retrieve a quality factor (Q) for this cavity of 20–30. Q is calculated as the ratio between the spectral width and the spectral position ($\Delta\lambda/\lambda$) of the cavity mode. [35,61] As suggested by its name, this finesse represents the quality of the microcavity. [35,61]

The value we retrieved is relatively small compared to other polymer microcavities that usually show values five to 10 times larger. However, this finesse is comparable to those of other solution processes' microcavities, such as those made of sintered metal oxide nanoparticles [35]. This similarity is probably due to the dissolution of the sacrificial layers upon (EDBE)PbCl$_4$ deposition which increases the film roughness. The effect of such roughness appears, however, comparable to that observed in the metal oxide nanoparticle multilayers that are successfully applied to a variety of fields, including sensing, [62] switchers, [44] and photon control in photovoltaics [6] (aside from lasing and light emission control [58,63–65]). On the other hand, polymer systems possess mechanical properties such as a level of flexibility that is inconceivable within inorganic structures [21,35,36,66].

4. Conclusions

We reported on the encapsulation of the broadband-emitting, perovskite-like (EDBE)PbCl$_4$ into polymer microcavities. We used sacrificial layers to circumvent the low compatibility of the (EDBE)PbCl$_4$ solvent (DMSO) and the polymeric structure underneath. With this strategy, we fully achieved a solution processed microcavity with a quality factor of about 20 and an optical behavior in agreement with theoretical predictions [35]. The photonic structure is able to modify the (EDBE)PbCl$_4$ emission profile over a broad spectral range. Despite a low level of finesse compared to other polymer structures, the performances of our system are comparable with those of other spun-cast inorganic photonic structures commonly employed in light management.

References

1. Zhang, W.; Saliba, M.; Moore, D.T.; Pathak, S.K.; Hörantner, M.T.; Stergiopoulos, T.; Stranks, S.D.; Eperon, G.E.; Alexander-Webber, J.A.; Abate, A.; et al. Ultrasmooth organic–inorganic perovskite thin-film formation and crystallization for efficient planar heterojunction solar cells. *Nat. Commun.* **2015**, *6*, 6142. [CrossRef] [PubMed]

2. NREL Research Cell Efficiency Records. Available online: https://www.nrel.gov/pv/cell-efficiency.html (accessed on 10 October 2019).

3. Gao, P.; Gratzel, M.; Nazeeruddin, M.K. Organohalide lead perovskites for photovoltaic applications. *Energy Environ. Sci.* **2014**, *7*, 2448–2463. [CrossRef]

4. Burschka, J.; Pellet, N.; Moon, S.-J.; Humphry-Baker, R.; Gao, P.; Nazeeruddin, M.K.; Gratzel, M. Sequential deposition as a route to high-performance perovskite-sensitized solar cells. *Nature* **2013**, *499*, 316–319. [CrossRef] [PubMed]

5. Zhou, H.; Chen, Q.; Li, G.; Luo, S.; Song, T.-B.; Duan, H.-S.; Hong, Z.; You, J.; Liu, Y.; Yang, Y. Interface engineering of highly efficient perovskite solar cells. *Science* **2014**, *345*, 542–546. [CrossRef] [PubMed]

6. Zhang, W.; Anaya, M.; Lozano, G.; Calvo, M.E.; Johnston, M.B.; Míguez, H.; Snaith, H.J. Highly efficient perovskite solar cells with tunable structural color. *Nano Lett.* **2015**, *15*, 1698–1702. [CrossRef]

7. Saliba, M.; Matsui, T.; Seo, J.-Y.; Domanski, K.; Correa-Baena, J.-P.; Nazeeruddin, M.K.; Zakeeruddin, S.M.; Tress, W.; Abate, A.; Hagfeldt, A.; et al. Cesium-containing triple cation perovskite solar cells: Improved stability, reproducibility and high efficiency. *Energy Environ. Sci.* **2016**, *9*, 1989–1997. [CrossRef]

8. Boix, P.P.; Agarwala, S.; Koh, T.M.; Mathews, N.; Mhaisalkar, S.G. Perovskite solar cells: Beyond methylammonium lead iodide. *J. Phys. Chem. Lett.* **2015**, *6*, 898–907. [CrossRef]

9. Saparov, B.; Mitzi, D.B. Organic–inorganic perovskites: Structural versatility for functional materials design. *Chem. Rev.* **2016**, *116*, 4558–4596. [CrossRef]

10. Cortecchia, D.; Neutzner, S.; Yin, J.; Salim, T.; Srimath Kandada, A.R.; Bruno, A.; Lam, Y.M.; Martí-Rujas, J.; Petrozza, A.; Soci, C. Structure-controlled optical thermoresponse in Ruddlesden-Popper layered perovskites. *APL Mater.* **2018**, *6*, 114207. [CrossRef]

11. Xing, G.; Mathews, N.; Lim, S.S.; Yantara, N.; Liu, X.; Sabba, D.; Grätzel, M.; Mhaisalkar, S.; Sum, T.C. Low-temperature solution-processed wavelength-tunable perovskites for lasing. *Nat. Mater.* **2014**, *13*, 476–480. [CrossRef]

12. Gil-Escrig, L.; Longo, G.; Pertegas, A.; Roldan-Carmona, C.; Soriano, A.; Sessolo, M.; Bolink, H.J. Efficient photovoltaic and electroluminescent perovskite devices. *Chem. Commun.* **2015**, *51*, 569–571. [CrossRef] [PubMed]

13. Chin, X.Y.; Cortecchia, D.; Yin, J.; Bruno, A.; Soci, C. Lead iodide perovskite light-emitting field-effect transistor. *Nat. Commun.* **2015**, *6*, 7383. [CrossRef]

14. Deschler, F.; Price, M.; Pathak, S.; Klintberg, L.E.; Jarausch, D.-D.; Higler, R.; Hüttner, S.; Leijtens, T.; Stranks, S.D.; Snaith, H.J.; et al. High photoluminescence efficiency and optically pumped lasing in solution-processed mixed halide perovskite semiconductors. *J. Phys. Chem. Lett.* **2014**, *5*, 1421–1426. [CrossRef] [PubMed]

15. Cho, H.; Jeong, S.-H.; Park, M.-H.; Kim, Y.-H.; Wolf, C.; Lee, C.-L.; Heo, J.H.; Sadhanala, A.; Myoung, N.; Yoo, S.; et al. Overcoming the electroluminescence efficiency limitations of perovskite light-emitting diodes. *Science* **2015**, *350*, 1222–1225. [CrossRef] [PubMed]

16. Cortecchia, D.; Mróz, W.; Neutzner, S.; Borzda, T.; Folpini, G.; Brescia, R.; Petrozza, A. Defect Engineering in 2D Perovskite by Mn(II) Doping for Light-Emitting Applications. *Chem* **2019**, *5*, 2146–2158. [CrossRef]

17. De Giorgi, M.L.; Anni, M. Amplified Spontaneous Emission and Lasing in Lead Halide Perovskites: State of the Art and Perspectives. *Appl. Sci.* **2019**, *9*, 4591. [CrossRef]

18. Perulli, A.; Balena, A.; Fernandez, M.; Nedelcu, G.; Cretí, A.; Kovalenko, M.V.; Lomascolo, M.; Anni, M. Full-color tuning in binary polymer:perovskite nanocrystals organic-inorganic hybrid blends. *Appl. Phys. Lett.* **2018**, *112*, 171904. [CrossRef]

19. Park, H.J.; Xu, T.; Lee, J.Y.; Ledbetter, A.; Guo, L.J. Photonic Color Filters Integrated with Organic Solar Cells for Energy Harvesting. *ACS Nano* **2011**, *5*, 7055–7060. [CrossRef]

20. Cortecchia, D.; Yin, J.; Bruno, A.; Lo, S.-Z.A.; Gurzadyan, G.G.; Mhaisalkar, S.; Bredas, J.-L.; Soci, C. Polaron self-localization in white-light emitting hybrid perovskites. *J. Mater. Chem. C* **2017**, *5*, 2771–2780. [CrossRef]

21. Lova, P.; Cortecchia, D.S.; Krishnamoorthy, H.N.; Giusto, P.; Bastianini, C.; Bruno, A.; Comoretto, D.; Soci, C. Engineering the Emission of Broadband 2D Perovskites by Polymer Distributed Bragg Reflectors. *ACS Photonics* **2018**, *5*, 867–874. [CrossRef]

22. Dohner, E.R.; Jaffe, A.; Bradshaw, L.R.; Karunadasa, H.I. Intrinsic white-light emission from layered hybrid perovskites. *J. Am. Chem. Soc.* **2014**, *136*, 13154–13157. [CrossRef]

23. Dou, L.; Wong, A.B.; Yu, Y.; Lai, M.; Kornienko, N.; Eaton, S.W.; Fu, A.; Bischak, C.G.; Ma, J.; Ding, T.; et al. Atomically thin two-dimensional organic-inorganic hybrid perovskites. *Science* **2015**, *349*, 1518–1521. [CrossRef]

24. Yin, J.; Li, H.; Cortecchia, D.; Soci, C.; Brédas, J.-L. Excitonic and polaronic properties of 2D hybrid organic–inorganic perovskites. *ACS Energy Lett.* **2017**, *2*, 417–423. [CrossRef]

25. Cortecchia, D.; Neutzner, S.; Srimath Kandada, A.R.; Mosconi, E.; Meggiolaro, D.; De Angelis, F.; Soci, C.; Petrozza, A. Broadband emission in two-dimensional hybrid perovskites: The role of structural deformation. *J. Am. Chem. Soc.* **2017**, *139*, 39–42. [CrossRef]

26. Cortecchia, D.; Yin, J.; Petrozza, A.; Soci, C. White light emission in low-dimensional perovskites. *J. Mater. Chem. C* **2019**, *7*, 4956–4969. [CrossRef]

27. Cortecchia, D.; Lew, K.C.; So, J.-K.; Bruno, A.; Soci, C. Cathodoluminescence of Self-Organized Heterogeneous Phases in Multidimensional Perovskite Thin Films. *Chem. Mater.* **2017**, *29*, 10088–10094. [CrossRef]

28. Gholipour, B.; Adamo, G.; Cortecchia, D.; Krishnamoorthy, H.N.S.; Birowosuto, M.D.; Zheludev, N.I.; Soci, C. Organometallic perovskite metasurfaces. *Adv. Mater.* **2017**, *29*, 1604268. [CrossRef]

29. Ramírez Quiroz, C.O.; Bronnbauer, C.; Levchuk, I.; Hou, Y.; Brabec, C.J.; Forberich, K. Coloring semitransparent perovskite solar cells via dielectric mirrors. *ACS Nano* **2016**, *10*, 5104–5112. [CrossRef]

30. Wang, J.; Cao, R.; Da, P.; Wang, Y.; Hu, T.; Wu, L.; Lu, J.; Shen, X.; Xu, F.; Zheng, G.; et al. Purcell effect in an organic-inorganic halide perovskite semiconductor microcavity system. *Appl. Phys. Lett.* **2016**, *108*, 022103. [CrossRef]

31. Yablonovitch, E. Inhibited spontaneous emission in solid-state physics and electronics. *Phys. Rev. Lett.* **1987**, *58*, 2059–2062. [CrossRef]

32. John, S. Strong localization of photons in certain disordered dielectric superlattices. *Phys. Rev. Lett.* **1987**, *58*, 2486–2489. [CrossRef]

33. Lova, P.; Soci, C. Nanoimprint Lithography: Toward Polymer Photonic Crystals. In *Organic and Hybrid Photonic Crystals*, 1st ed.; Comoretto, D., Ed.; Springer: Cham, Switzerland, 2015; Volume 1, p. 493.

34. Comoretto, D. (Ed.) *Organic and Hybrid Photonic Crystals*, 1st ed.; Springer International Publishing: Cham, Switzerland, 2015; Volume XXI, p. 497.

35. Lova, P.; Manfredi, G.; Comoretto, D. Advances in Functional Solution Processed Planar One-Dimensional Photonic Crystals. *Adv. Opt. Mater.* **2018**, *6*, 1800726–1800730. [CrossRef]

36. Iasilli, G.; Francischello, R.; Lova, P.; Silvano, S.; Surace, A.; Pesce, G.; Alloisio, M.; Patrini, M.; Shimizu, M.; Comoretto, D.; et al. Luminescent Solar Concentrators: Boosted Optical Efficiency by Polymer Dielectric Mirrors. *Mater. Chem. Front.* **2019**, *3*, 429–436. [CrossRef]

37. Lova, P.; Manfredi, G.; Bastianini, C.; Mennucci, C.; Buatier de Mongeot, F.; Servida, A.; Comoretto, D. Flory-Huggins Photonic Sensors for the Optical Assessment of Molecular Diffusion Coefficients in Polymers. *ACS Appl. Mater. Interfaces* **2019**, *11*, 16872–16880. [CrossRef]

38. Giusto, P.; Lova, P.; Manfredi, G.; Gazzo, S.; Srinivasan, B.; Radice, S.V.; Comoretto, D. Colorimetric Detection of Perfluorinated Compounds by All-Polymer Photonic Transducers. *ACS Omega* **2018**, *3*, 7517–7522. [CrossRef]

39. Lova, P. Selective Polymer Distributed Bragg Reflector Vapor Sensors. *Polymers* **2018**, *10*, 1161. [CrossRef]

40. Lova, P.; Comoretto, D. Label-free vapor selectivity by polymer-inorganic composite photonic crystals sensors. *AIP Conf. Proc.* **2018**, *1981*, 020097.

41. Lova, P.; Bastianini, C.; Giusto, P.; Patrini, M.; Rizzo, P.; Guerra, G.; Iodice, M.; Soci, C.; Comoretto, D. Label-free Vapor Selectivity in Poly(p-phenylene oxide) Photonic Crystal Sensors. *ACS Appl. Mater. Interfaces* **2016**, *8*, 31941–31950. [CrossRef]

42. Paternò, G.M.; Moscardi, L.; Donini, S.; Ariodanti, D.; Kriegel, I.; Zani, M.; Parisini, E.; Scotognella, F.; Lanzani, G. Hybrid One-Dimensional Plasmonic–Photonic Crystals for Optical Detection of Bacterial Contaminants. *J. Phys. Chem. Lett.* **2019**, *10*, 4980–4986. [CrossRef]

43. Kriegel, I.; Scotognella, F. Light-induced switching in pDTE–FICO 1D photonic structures. *Opt. Commun.* **2018**, *410*, 703–706. [CrossRef]

44. Paternò, G.M.; Iseppon, C.; D'Altri, A.; Fasanotti, C.; Merati, G.; Randi, M.; Desii, A.; Pogna, E.A.A.; Viola, D.; Cerullo, G.; et al. Solution Processable and Optically Switchable 1D Photonic Structures. *Sci. Rep.* **2018**, *8*, 3517. [CrossRef]

45. Paternò, G.M.; Moscardi, L.; Kriegel, I.; Scotognella, F.; Lanzani, G. Electro-optic and magneto-optic photonic devices based on multilayer photonic structures. *J. Photonics Energy* **2018**, *8*, 032201. [CrossRef]

46. Scotognella, F.; Varo, S.; Criante, L.; Gazzo, S.; Manfredi, G.; Knarr, R.J., III; Comoretto, D. Spin-Coated Polymer and Hybrid Multilayers and Microcavities. In *Organic and Hybrid Photonic Crystals*, 1st ed.; Comoretto, D., Ed.; Springer: Cham, Switzerland, 2015; Volume 1, p. 493.

47. Canazza, G.; Scotognella, F.; Lanzani, G.; De Silvestri, S.; Zavelani-Rossi, M.; Comoretto, D. Lasing from all-polymer microcavities. *Laser Phys. Lett.* **2014**, *11*, 035804. [CrossRef]

48. Scotognella, F.; Monguzzi, A.; Cucini, M.; Meinardi, F.; Comoretto, D.; Tubino, R. One dimensional polymeric organic photonic crystals for DFB lasers. *Int. J. Photoenergy* **2008**, *2008*, 389034. [CrossRef]

49. Frezza, L.; Patrini, M.; Liscidini, M.; Comoretto, D. Directional Enhancement of Spontaneous Emission in Polymer Flexible Microcavities. *J. Phys. Chem. C* **2011**, *115*, 19939–19946. [CrossRef]

50. Gazzo, S.; Manfredi, G.; Pötzsch, R.; Wei, Q.; Alloisio, M.; Voit, B.; Comoretto, D. High refractive index hyperbranched polyvinylsulfides for planar one-dimensional all-polymer photonic crystals. *J. Polym. Sci. Part B Polym. Phys.* **2016**, *54*, 73–80. [CrossRef]

51. Knarr, R.J., III; Manfredi, G.; Martinelli, E.; Pannocchia, M.; Repetto, D.; Mennucci, C.; Solano, I.; Canepa, M.; Buatier de Mongeot, F.; Galli, G.; et al. In-plane anisotropic photoresponse in all-polymer planar microcavities. *Polymer* **2016**, *84*, 383–390. [CrossRef]

52. Fornasari, L.; Floris, F.; Patrini, M.; Comoretto, D.; Marabelli, F. Demonstration of fluorescence enhancement via bloch surface waves in all-polymer multilayer structures. *Phys. Chem. Chem. Phys.* **2016**, *18*, 14086–14093. [CrossRef]

53. Manfredi, G.; Mayrhofer, C.; Kothleitner, G.; Schennach, R.; Comoretto, D. Cellulose Ternary Photonic Crystal created by Solution Processing. *Cellulose* **2016**, *23*, 2853–2862. [CrossRef]

54. Manfredi, G.; Lova, P.; Di Stasio, F.; Krahne, R.; Comoretto, D. Directional Fluorescence Spectral Narrowing in All-Polymer Microcavities Doped with CdSe/CdS Dot-in-rod Nanocrystals. *ACS Photonics* **2017**, *4*, 1761–1769. [CrossRef]

55. Lova, P.; Grande, V.; Manfredi, G.; Patrin, M.; Herbst, S.; Würthner, F.; Comoretto, D. All-Polymer Photonic Microcavities Doped with Perylene Bisimide J-Aggregates. *Adv. Opt. Mater.* **2017**, *5*, 1700523. [CrossRef]

56. Manfredi, G.; Lova, P.; Di Stasio, F.; Rastogi, P.; Krahne, R.; Comoretto, D. Lasing From Dot-In-Rod Nanocrystals in Planar Polymer Microcavities. *RSC Adv.* **2018**, *8*, 13026–13033. [CrossRef]

57. Monguzzi, A.; Scotognella, F.; Meinardi, F.; Tubino, R. Lasing in one dimensional dye-doped random multilayer. *Phys. Chem. Chem. Phys.* **2010**, *12*, 12947–12950. [CrossRef]

58. Scotognella, F.; Puzzo, D.P.; Zavelani-Rossi, M.; Clark, J.; Sebastian, M.; Ozin, G.A.; Lanzani, G. Two-photon poly(phenylenevinylene) DFB laser. *Chem. Mater.* **2011**, *23*, 805–809. [CrossRef]

59. Lova, P.; Giusto, P.; Stasio, F.D.; Manfredi, G.; Paternò, G.M.; Cortecchia, D.; Soci, C.; Comoretto, D. All-Polymer Methylammonium Lead Iodide Perovskite Microcavity. *Nanoscale* **2019**, *11*, 8978–8983. [CrossRef]

60. Radice, S.V.; Srinivasan, P.; Comoretto, D.; Gazzo, S. One-Dimensional Planar Photonic Crystals Including Fluoropolymer Compositions and Corresponding Fabrication Methods. WO 2016/087439 A1, 9 June 2016.

61. Joannopoulos, J.D.; Johnson, S.G.; Winn, J.N.; Meade, R.D. *Photonic Crystals: Molding the Flow of Light*; Princeton University Press, Woodstock: Princeton, NJ, USA, 2011.

62. Bonifacio, L.D.; Ozin, G.A.; Arsenault, A.C. Photonic nose–sensor platform for water and food quality control. *Small* **2011**, *7*, 3153–3157. [CrossRef]

63. Scotognella, F.; Monguzzi, A.; Meinardi, F.; Tubino, R. DFB laser action in a flexible fully plastic multilayer. *Phys. Chem. Chem. Phys.* **2010**, *12*, 337–340. [CrossRef]

64. Puzzo, D.P.; Scotognella, F.; Zavelani-Rossi, M.; Sebastian, M.; Lough, A.J.; Manners, I.; Lanzani, G.; Tubino, R.; Ozin, G.A. Distributed feedback lasing from a composite poly(phenylene vinylene)−nanoparticle one-dimensional photonic crystal. *Nano Lett.* **2009**, *9*, 4273–4278. [CrossRef]

65. Scotognella, F.; Puzzo, D.P.; Monguzzi, A.; Wiersma, D.S.; Maschke, D.; Tubino, R.; Ozin, G.A. Nanoparticle one-dimensional photonic-crystal dye laser. *Small* **2009**, *5*, 2048–2052. [CrossRef]

66. Lova, P.; Manfredi, G.; Boarino, L.; Laus, M.; Urbinati, G.; Losco, T.; Marabelli, F.; Caratto, V.; Ferretti, M.; Castellano, M.; et al. Hybrid ZnO:Polystyrene Nanocomposite for All-Polymer Photonic Crystals. *Phys. Status Solidi C* **2015**, *12*, 158–162. [CrossRef]